AIChE

Alternative Concept for SOFC with Direct Internal Reforming Operation: Benefits from Inserting Catalyst Rod

Pannipha Dokamaingam and Navadol Laosiripojana
Energy Division, The Joint Graduate School of Energy and Environment, King Mongkut's University of Technology Thonburi, Bangkok 10140, Thailand

Apinan Soottitantawat and Suttichai Assabumrungrat
Dept. of Chemical Engineering, Faculty of Engineering, Chulalongkorn University, Bangkok 10330, Thailand

DOI 10.1002/aic.12091
Published online October 20, 2009 in Wiley InterScience (www.interscience.wiley.com).

Mathematical models of direct internal reforming solid oxide fuel cell (DIR-SOFC) fueled by methane are developed using COMSOL® software. The benefits of inserting Ni-catalyst rod in the middle of tubular-SOFC are simulated and compared to conventional DIR-SOFC. It reveals that DIR-SOFC with inserted catalyst provides smoother temperature gradient along the system and gains higher power density and electrochemical efficiency with less carbon deposition. Sensitivity analyses are performed. By increasing inlet fuel flow rate, the temperature gradient and power density improve, but less electrical efficiency with higher carbon deposition is predicted. The feed with low inlet steam/carbon ratio enhances good system performances but also results in high potential for carbon formation; this gains great benefit of DIR-SOFC with inserted catalyst because the rate of carbon deposition is remarkably low. Compared between counter- and co-flow patterns, the latter provides smoother temperature distribution with higher efficiency; thus, it is the better option for practical applications.
 AIChE J, 56: 1639–1650, 2010
Keywords: direct internal reforming, solid oxide fuel cell, catalyst

Introduction

Solid oxide fuel cell (SOFC) is an electrochemical device that typically operated at high temperature (973–1373 K)[1,2]; this technology is expected to be applied for energy generation in the near future. SOFC offers several advantages, e.g., the ability to use CO (along with H_2) as fuel and the high level of exhaust heat, which can be efficiently used in combined heat and power and combined cycle gas turbine applications. Importantly, because of its high operating temperature, several hydrocarbon compounds could be applied as primary fuels when it is operated as internal reforming (IR-SOFC). Currently, methane (as a major component in natural gas) is the most common primary fuel for IR-SOFC.

According to the internal reforming, this operation is referred to as the utilization of heat generated from exothermic electrochemical reaction to endothermic (steam) reforming of hydrocarbons.[2–5] Theoretically, there are two approaches for IR-SOFC, i.e., direct internal reforming (DIR-SOFC) and indirect internal reforming (IIR-SOFC). For DIR-SOFC approach, along with electrochemical reaction, the reforming reaction occurs simultaneously at the anode side of SOFC. Thus, high heat transfer and fuel conversion can be achieved from this operation; nevertheless, anode material must be optimized for both reactions and could be easily poisoned by carbon deposition from the reforming

Correspondence concerning this article should be addressed to N. Laosiripojana at navadol_l@jgsee.kmutt.ac.th.

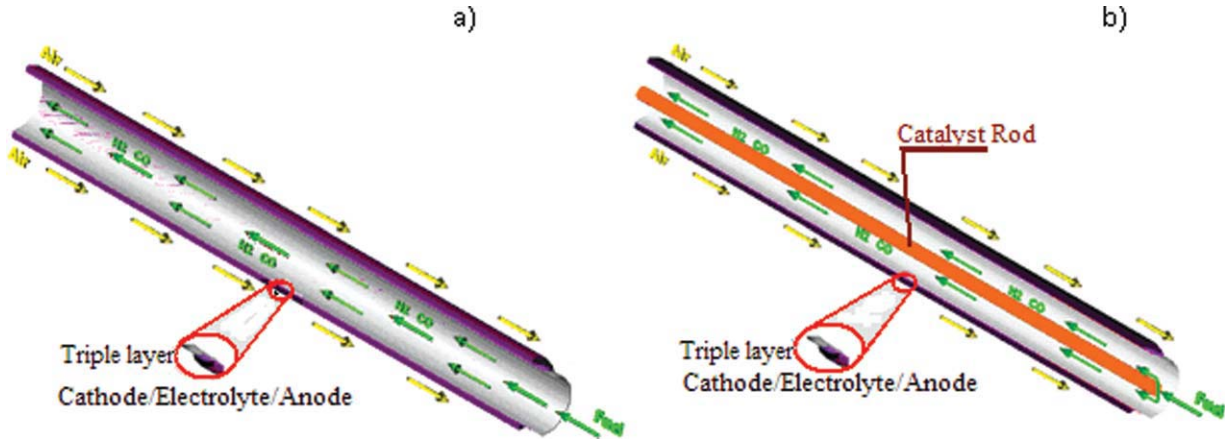

Figure 1. Tubular-designed DIR-SOFC systems in this work.

(a) Conventional DIR-SOFC and (b) inserted catalyst rod DIR-SOFC. [Color figure can be viewed in the online issue, which is available at www.interscience.wiley.com.]

of hydrocarbons. As for IIR-SOFC, the endothermic reforming reaction takes place at a reformer, which is in close thermal contact with the anode side of SOFC where exothermic electrochemical reaction occurs. IIR-SOFC gives advantage in terms of eliminating the requirement of separate fuel reformer and preventing anode material from carbon deposition. Nevertheless, IIR-SOFC offers less fuel conversion and also requires complex configuration compared to DIR-SOFC. Importantly, another major drawback of both DIR and IIR operation is the possible mismatch between rates of endothermic and exothermic reactions, which leads to significant local temperature reduction particularly near the entrance of the anode channel (for DIR) or reformer channel (for IIR) and consequently results in mechanical failure due to thermally induced stresses.[3–7]

In this work, a set of mathematical models was developed to predict the behaviors of tubular-designed DIR-SOFC fueled by methane, i.e., cell performance, temperature gradient, and amount of carbon deposition along the cell. The developed model was coded in COMSOL® program within 2D axial dimension application with an aim of determining the effect of operating conditions, i.e., inlet steam to carbon ratio and gas flow pattern on the system performance. Importantly, as the main scope of this study, we proposed one alternative concept for DIR-SOFC by investigating the benefits of inserting catalyst rod in the middle of the fuel channel. This configuration can be called as a hybrid system between DIR and IIR operations because the reforming reaction takes place simultaneously with the electrochemical reaction at the anode (as DIR operation) and also occurs on separate internal reforming catalyst (as IIR operation). It is noted that the intrinsic rate equations of methane steam reforming and the rate of carbon formation over Ni-based material as reported by Xu and Froment[8] and Zavarukhin and Kuvshinov[9] were applied integrally with DIR-SOFC model to predict the reforming characteristics of "Ni-based" catalyst rod and anode along with the electrochemical behavior of SOFC system. Details of these mathematical models are presented in the next section.

From the simulation, the system performances (i.e., electrical efficiency, temperature gradient along the cell, and amount of carbon formation at anode surface) of this DIR-SOFC with catalyst rod were determined. The effects of inlet steam to carbon ratio and gas flow patterns on the performance of this DIR-SOFC were also investigated and compared to conventional DIR-SOFC. Lastly, the suitable operating conditions of DIR-SOFC system fueled by methane were identified.

Mathematical Models

Model geometry

The schematic diagram of a tubular-designed DIR-SOFC applied in this work is shown in Figure 1. As described, two configurations, i.e., conventional tubular DIR-SOFC (Figure 1a) and DIR-SOFC with inserted catalyst rod (Figure 1b) were considered. For both configurations, methane and steam are fed to the anode channel of SOFC, where they were simultaneously converted to hydrogen-rich gas along with consumed electrochemically to generate electricity. Simultaneously, air is fed with the opposite flow direction through the air channel. It is noted that anode/electrolyte/cathode compositions of SOFC system considered here are Ni-YSZ/YSZ/LSM. All dimensions and physical properties of this SOFC system, which are based on the previous report from literatures,[10–14] are summarized in Table 1.

Model assumption and equations

The model was developed as the smallest single unit cell taking into account the effect of temperature on gas distribution, reactant conversion, and charge transfer. Our developed models were based on these assumptions: (1) each section is considered as nonisothermal steady-state conditions, (2) ideal gas behavior is applied for all gas components, (3) pressure drop in SOFC stack was neglected, (4) fuel utilization was fixed constantly at 80%, and (5) the reforming reaction and carbon formation occurred at the surface of Ni particles on the catalyst rod and SOFC anode. It is noted that the well-established methane steam reforming rate expressions proposed by Xu and Forment[8] were applied to predict the reforming rate for both sections; the difference in steam

Table 1. Constant Parameter Values of a Tubular IIR-SOFC System

Parameter	Value	Reference
Fuel cell length	0.60 m	10
Inserted catalyst rod	2×10^{-3} m	–
Inside radius of the cell	5.4×10^{-3} m	10
Anode thickness	1×10^{-3} m	10
Electrolyte thickness	4×10^{-5} m	10
Cathode thickness	5×10^{-5} m	10
Anode permeability	1×10^{-12}	11
Cathode permeability	1×10^{-12}	11
Average density of triple phase	633.73 kg m^{-3}	14
Average specific heat of triple phase	574.3 J kg^{-1} K^{-1}	14
Anode thermal conductivity	6.23 W m^{-1} K^{-1}	14
Electrolyte conductivity	2.7 W m^{-1} K^{-1}	14
Cathode thermal conductivity	9.6 W m^{-1} K^{-1}	14
Convection coefficient in the fuel channel	2987 W m^{-2} K^{-1}	14
Convection coefficient in the air channel	1322.8 W m^{-2} K^{-1}	14

reforming reactivity between them is related to the dissimilarity of their Ni-active surface area. In our modeling, the dimensions of SOFC system were modified to dimensionless application (with the full scale of 1.0), and the active areas of catalyst rod and anode were normalized as relative active area. The relative active surface area of anode is 0.07, whereas that of catalyst rod is 0.36. A number of equations were applied to predict concentration and temperature gradients along this tubular DIR-SOFC system. Details for these sets of equations are presented in the following sections and summarized in Table 2.

Gas Distribution. The combination of Brinkman equation and Navier-Stokes equation[15] (Eq. 1) was applied to predict gases distribution behavior in this work:

$$\nabla \cdot (\rho u u) = -\nabla p + \nabla \cdot (\nabla \mu u) - \frac{\mu}{k_p}(\varepsilon u), \tag{1}$$

where u is the fluid velocity, ρ the density, p the pressure, μ the viscosity, ε the porosity, and k_p is the permeability. It is noted that the influences of pressure and velocity gradient on gas diffusion properties were also took into account by applying molecular diffusion and binary diffusion equations (Eqs. 2 and 3, respectively).[16]

$$D_{i,\mathrm{mix}} = (1 - y_i) / \sum_{j,j \neq 1} (y_j / D_{ij}) \tag{2}$$

$$D_{i,j} = (0.00143) T^{1.75} / p M_{i,j}^{1/2} [\gamma_i^{1/3} + \gamma_j^{1/3}]^2, \tag{3}$$

where $D_{i,\mathrm{mix}}$ and $D_{i,j}$ are molecular diffusion and binary diffusion flux of species i in mixed gas (m^2 s^{-1}), y_i is mole fraction of species i, p is pressure, $M_{i,j} = 2/(1/M_i + 1/M_j$ in which M_i is molecular weight of component i, and γ is the special diffusion volume as reported by Fuller et al.[17] It is noted that, in the case of porous media, the diffusion behavior was corrected by applying porosity (ε) and tortuosity (τ), so-called effective diffusivity coefficient $D^{\mathrm{e}}_{i,\mathrm{pmix}}$ (Eq. 4). Furthermore, gas diffusion through porous media, $D_{i,\mathrm{pmix}}$, was explained by two mechanisms, i.e., molecular diffusion ($D_{i,\mathrm{mix}}$) (Eq. 5) and Knudsen diffusion ($D_{i,\mathrm{ku}}$) (Eq. 6) depending on the relation between pore diameter (d_{p}) and mean free path of molecular species.

$$D^{\mathrm{e}}_{i,\mathrm{pmix}} = \frac{\varepsilon}{\tau} D_{i,\mathrm{pmix}} \tag{4}$$

$$\frac{1}{D_{i,\mathrm{pmix}}} = \frac{1}{D_{i,\mathrm{mix}}} + \frac{1}{D_{i,\mathrm{ku}}} \tag{5}$$

$$D_{i,\mathrm{ku}} = \frac{1}{3} d_{\mathrm{p}} \sqrt{\frac{8RT}{\pi M_i}}, \tag{6}$$

where R is universal gas constant.

Energy Transfer. Heat transfer phenomena considered in this system involve the conduction along stack materials and convection from heat flow though the system. Furthermore, the effect of heat radiation between the catalyst rod and SOFC was also concerned for the case of DIR-SOFC with inserted catalyst rod. The calculated gas properties were referred as a function of temperature; thus, momentum, mass, and energy balances were integrated. It should be noted that, in all gas flow channels, both conduction and convection heat transfers were considered, and the heat capacity and conductivity of gas species were set as the function of temperature.[16]

Reforming Model. As mentioned earlier, methane steam reforming reaction over Ni-based catalyst rod and SOFC anode was simulated based on the intrinsic rate equations and parameters reported by Xu and Froment,[8] whereas the amount of carbon deposition was predicted based on the equations proposed by Zavarukhin and Kuvshinov.[9] It is noted that the developed model for predicting the rate of carbon formation, which was coded in COMSOL® program in this work, was first validated with the results reported by Zavarukhin and Kuvshinov[9] at the same operating conditions. As shown in Figure 2a, both results are in good agreement with the error less than 5%.

Importantly, the effects of heat convection in gas stream, heat of reactions, and conductive heat transfers from fuel channel were taken into account in the reforming model. Furthermore, in the case of DIR-SOFC with inserted catalyst rod, the radiation between the catalyst rod and the solid cell was also considered. We made the assumption here that the reforming reactions occurred only at the catalyst surface, and no gas was diffused into the catalyst rod.

SOFC Model. All momentum, mass, heat, and charge balance equations for SOFC systems in this work are given in Table 2. In detail, all electrochemical reactions take place at electrodes and electrolyte interface to generate electricity from both H_2 and CO. Here, the cell voltage is theoretically calculated from Nernst equation. It is noted that the actual voltage is always less than the theoretical value because of the presence of activation, concentration, and ohmic overpotentials.[1,2]

Activation loss

Activation loss, η_{act}, is the activation barrier of electrochemical reaction at electrode, which is significant at low current density.[2] This overpotential is determined from Butler-Volmer equation, Eq. 7. The relations of current density with H_2 and O_2 concentrations at electrodes are given in

Eqs. 8 and 9.[18] As the expression of activation loss from CO oxidation is not well ascertained, the current density from CO is assumed to be three times lower than that from H_2 (Eq. 10).[19] It is noted that all parameter values related to these equations are reported in Table 3.

$$j = j_0\left[\exp\left(\alpha\frac{n_e F}{RT}\eta_{act}\right) - \exp\left((1-(1-\alpha)\frac{n_e F}{RT}\eta_{act}\right)\right] \quad (7)$$

$$j_{0,H_2} = \vartheta_{anode}\left(\frac{p_{H_2}}{p_{ref}}\right)\left(\frac{p_{H_2O}}{p_{ref}}\right)\exp\left(-\frac{E_{act,anode}}{RT}\right) \quad (8)$$

$$j_{0,O_2} = \vartheta_{cathode}\left(\frac{p_{O_2}}{p_{ref}}\right)^{0.25}\exp\left(-\frac{E_{act,cathode}}{RT}\right) \quad (9)$$

$$j_{0,CO} = \frac{1}{3}j_{0,H_2}, \quad (10)$$

where j_0 is the exchange current density, j the current density, ϑ the exchange current density constant, α the charge transfer coefficient, n_e the number of electron, F the Faraday's constant and E_{act} is the activation energy.

Concentration overpotential

This overpotential, η_{con}, is caused by the dropping of pressure or partial pressure of reactant gases along porous electrodes at reaction sites.[2] It is normally reduced at high current density. The diffusion at bulk zone as defined in term of concentration overpotential is given in Eq. 11.[20,21] According to Suwanwarangkul et al.[22] and Hernández-Pacheco et al.,[23] the dusty gas model was applied to calculate concentration at active site.

$$\eta_{con} = \frac{RT}{2F}\ln\left(\frac{p^*_{H_2}p_{H_2O}}{p_{H_2}p^*_{H_2O}}\right) + \frac{RT}{2F}\ln\left(\frac{p^*_{CO}p_{CO_2}}{p_{CO}p^*_{CO_2}}\right) + \frac{RT}{4F}\ln\left(\frac{p^*_{O_2}}{p_{O_2}}\right), \quad (11)$$

where * represents gas partial pressure at active site.

Ohmic overpotential

This overpotential, η_{ohm}, occurs from the ion transport across the cell, which mainly depends on ionic conductivity of cell material. By applying ohm's law, the relation of ohmic overpotential and material resistivity is given in Eqs. 12 and 13,[12] in which the resistivity is determined from Eq. 14 based on the data in Table 4.

$$\eta_{ohm} = jR_{ohm} \quad (12)$$

$$R_{ohm} = \frac{\omega\delta}{A_{elec}} \quad (13)$$

$$\omega = a\cdot\exp(b/T), \quad (14)$$

where R_{ohm} is the ohmic resistance, ω the ionic conductivity, δ the thickness of electrode or electrolyte layer, and a,b are the constant property of material. It is noted that the transmission-line model as reported by Stiller et al.[24] can also apply to estimate the ohmic overpotential with comparable results to these equations. By applying the operating conditions (e.g., pressure, air, and fuel flow rates, inlet fuel temperature, fuel utilization, and inlet fuel composition) based on the work of Stiller et al.,[24] the deviations of observed ohmic overpotential between both models are in the range of ±6% (within the operating temperature range of 1250–1350 K).

Considering all polarizations, the cell performance was determined in terms of the electrical efficiency. It is noted that the anodic current was calculated from both H_2 and CO conversion rates, whereas the cell efficiency, η_{elec}, was calculated from the ratio between output power density (P) and the energy of all input fluids, Eq. 15.

$$\eta_{elec} = \frac{P.A_{act}}{\sum y_i^{in}LHV_{i,1173K}}, \quad (15)$$

where A_{act} is the activation area, (m^2), $LHV_{i,1173k}$ the lower heating value of component i at 1173 K., P the power density (W cm^{-2}), and y_i^{in} is the mole fraction of inlet gas, i. The governing equations for mass and heat transfers of SOFC anode are summarized in Table 2. It should be noted that I–V curve obtained from developed model in this work was validated with the previous work of Leng et al., [13] as shown in Figure 2b. Clearly, both the results are in good agreement.

Results and Discussion

Modeling of conventional DIR-SOFC and DIR-SOFC with inserted catalyst rod

The tubular DIR-SOFC model (with and without inserted catalyst rod) was first simulated at 1173 K and 1 bar. The inlet fuel (methane and steam) with inlet steam to carbon (S/C) ratio of 2 was fed to the fuel channel with a total flow rate of 24.8 $cm^3\ s^{-1}$; simultaneously, air was introduced to the cathode channel with the flow rate of 94.24 $cm^3\ s^{-1}$ (theoretical oxygen ratio). Table 3 presents all related parameters of these DIR-SOFC systems. It is noted that the consumption rate of H_2 and CO (U_f) at the anode channel was fixed constant at 80% for both configurations. Under these conditions, characteristic results of these two DIR-SOFC configurations, i.e., methane conversion, product gas distribution, and temperature gradient along SOFC channels (both fuel and air channels) are shown in Figures 3 and 4.

Figures 3a,b present the mole profiles of methane and hydrogen along the fuel channel of conventional DIR-SOFC (without inserted catalyst rod). It can be seen that the concentration of methane decreased along the length of fuel channel particularly at the surface of the anode (on the right-hand side of the channel); nevertheless, it is clear that significant amount of methane remains unreacted and presented at the outlet of the fuel channel. As for hydrogen concentration profile, oppositely, it increased along the length of fuel channel particularly at the surface of the anode, and considerable amount of hydrogen was presented in the gas products at the exit of the fuel channel. Both figures indicated that, under conventional DIR-SOFC conditions, methane incompletely reformed and hydrogen was inefficiently used by electrochemical reaction.

Figures 3c,d show the mole profiles of methane and hydrogen along the fuel channel of DIR-SOFC with inserted catalyst rod. Clearly, significant improvements in methane conversion and hydrogen utilization can be achieved. In detail,

Table 2. Steady-State 2D Dimensional Model's for Tubular DIR-SOFC

Fuel channel for conventional DIR-SOFC

$$\text{Mass balance } \nabla.(-D_i\nabla_{c_i} + c_i\vec{v}) = 0 \tag{17}$$

$$\text{Energy balance } \nabla.(\vec{v}\rho c_p T) - \sum \nabla.(\lambda_i \nabla T) = 0 \tag{18}$$

Boundary

$$z = L;\ r \geq 0;\ u_f = u_{in},$$
$$v_f = v_{in}, p_f = p_r, c_{i,f} = c_{i,in}, T_f = T_{in}$$

Fuel/anode interface and

$$\begin{aligned} z \geq 0; \quad & \mathbf{n}\cdot N_{CH_4,f} = -\sum R_{reform} - R_{c-from}, \\ & \mathbf{n}\cdot N_{H_2O,f} = -\sum R_{reform} \\ & \mathbf{n}\cdot N_{H_2,f} = \sum R_{reform} + R_{c-from}, \\ & \mathbf{n}\cdot N_{CO,f} = -\sum R_{reform} \\ & \mathbf{n}\cdot N_{CO_2} = \sum R_{reform} \\ & \mathbf{n}\cdot(k\nabla T) = h(T_f - T_s) + \sum \nabla H_{reform} R_{reform} \end{aligned}$$

Anode/electrolyte 1 interface

$$\begin{aligned} z \geq 0; \ & \mathbf{n}\cdot N_{H_2,f} = -J_{H_2}/2F, \\ & \mathbf{n}\cdot N_{H_2O,f} = J_{H_2}/2F \\ & \mathbf{n}\cdot N_{CO,f} = -J_{CO}/2F,, \\ & \mathbf{n}\cdot N_{CO_2,f} = J_{CO}/2F \\ & \mathbf{n}\cdot(k\nabla T) = \sum \Delta H_{elec} R_{elec} + J(E - \eta_{total}) \end{aligned}$$

Fuel channel for inserted catalyst rod DIR-SOFC

$$\text{Mass balance } \quad \nabla.(-D_i\nabla c_i + c_i\vec{v}) = 0 \tag{19}$$

$$\text{Energy balance } \nabla.(\vec{v}\rho c_p T) - \sum \nabla.(\lambda_i \nabla T) = 0 \tag{20}$$

Boundary

$$z = L;\ r \geq 0;\ u_f = u_{in}, v_f = v_{in},$$
$$p_f = p_r, c_{i,f} = c_{i,in}, T_f = T_{in}, T_{rod} = T_{in}$$

Fuel/catalyst rod interface and fuel/anode interface

$$\begin{aligned} z \geq 0; \quad & \mathbf{n}\cdot N_{CH_4,f} = -\sum R_{reform} - R_{c-from}, \\ & \mathbf{n}\cdot N_{H_2O,f} = -\sum R_{reform} \\ & \mathbf{n}\cdot N_{H_2,f} = \sum R_{reform} + R_{c-from}, \\ & \mathbf{n}\cdot N_{CO,f} = -\sum R_{reform} \\ & \mathbf{n}\cdot N_{CO_2} = \sum R_{reform} \end{aligned}$$

(*Continued*)

Table 2. (Continued)

Fuel/catalyst rod interface

$$\mathbf{n}\cdot(k\nabla T) = h_f(T_{rod} - T_f) + \sum \Delta H_{reform} R_{reform} + \frac{\sigma A_s (T_r^4 - T_s^4)}{\frac{1}{\varepsilon_r} + \frac{A_r}{A_s}\left(\frac{1}{\varepsilon_s} - 1\right)}$$

Fuel/anode interface

$$\mathbf{n}\cdot(k\nabla T) = h(T_f - T_s) + \sum \Delta H_{reform} R_{reform}$$

Anode/electrolyte 1 interface

$$\begin{aligned} z \geq 0; \quad & \mathbf{n}\cdot N_{H_2,f} = -J_{H_2}/2F, \\ & \mathbf{n}\cdot N_{H_2O,f} = J_{H_2}/2F \\ & \mathbf{n}\cdot N_{CO,f} = -J_{CO}/2F, \\ & \mathbf{n}\cdot N_{CO_2,f} = J_{CO}/2F \\ & \mathbf{n}\cdot(k\nabla T) = \sum \Delta H_{elec} R_{elec} + J\eta_{total} \end{aligned}$$

Solid cell

$$\text{Energy balance } \nabla.(\vec{v}\rho c_p T) - \nabla.(\lambda_s \nabla T) + \sum \Delta H_{elec} + \frac{\sigma A_s (T_r^4 - T_s^4)}{\frac{1}{\varepsilon_r} + \frac{A_r}{A_s}\left(\frac{1}{\varepsilon_s} - 1\right)} = 0 \tag{21}$$

Boundary

$$z = L;\ r \geq 0;\ T_s = T_{in}$$

Air channel

$$\text{Mass balance } \nabla.(-D_i\nabla c_i + c_i\vec{v}) = 0 \tag{22}$$

$$\nabla.(\vec{v}\rho c_p T) - \Sigma\nabla.(\lambda_i \nabla T) = 0 \tag{23}$$

Boundary

$$z = 0;\ r \geq 0; \quad u_a = 0, v_a = v_{a,in}, c_{i,a} = c_{a,in},\ T_a = T_{a,in}$$

Air/cathode interface

$$\begin{aligned} z \geq 0; \quad & \mathbf{n}\cdot N_{O_2,f} = -J_{O_2}/2F \\ & \mathbf{n}\cdot(k\nabla T) = h(T_s - T_a) \end{aligned}$$

Outer layer

$$z \geq 0 \quad \mathbf{n}\cdot(k\nabla T) = 0$$

as seen in Figure 3c, the concentration of methane decreased along the length of fuel channel particularly near the anode and catalyst rod with greater rate than conventional DIR-SOFC because of the promotion of reforming reactivity by inserting the catalyst rod. Importantly, as shown in Figure 3d, hydrogen generated from the steam reforming reaction was

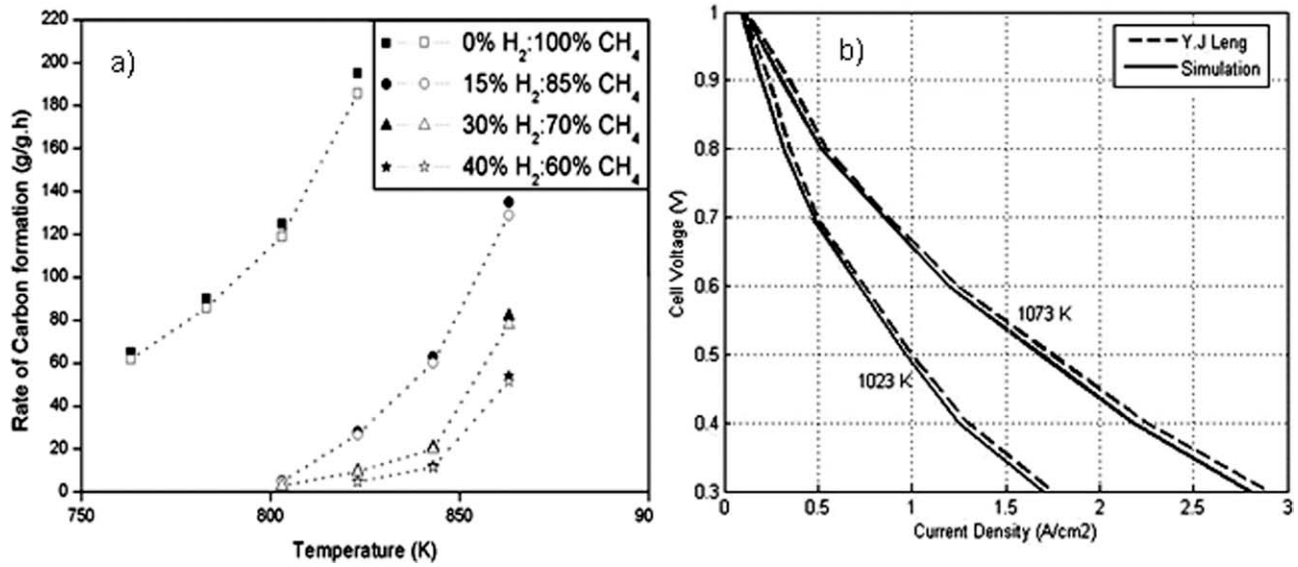

Figure 2. Validations of simulation results in this work with the literature.[9,13]

(a) Rate of carbon formation at various conditions (our simulation: blank symbols and the results from the literature[9]: black symbols); (b) *I–V* curve validation between our simulation results with the experimental results from literatures.[13]

efficiently used along the channel, thus significantly lower amount of hydrogen left the system compared to the conventional DIR-SOFC system. The results from Figures 3a–d can be summarize that, without catalyst rod, the anode alone inefficiently reforms methane, thus significant amount of methane remains presented in the system; under methane-rich gas condition, hydrogen generated from the reforming reaction cannot be well utilized electrochemically. By inserting the catalyst rod, the steam reforming of methane was promoted; with less methane presented in the system, hydrogen can be efficiently used via electrochemical reaction.

Figure 4 presents the temperature profiles along the fuel and air channels of both DIR-SOFC systems. Obviously, the local temperature reduction at the entrance of the fuel channel was reduced, and smoother temperature profiles along both channels can be achieved when the catalyst rod was inserted into the fuel channel. The temperature of DIR-SOFC with inserted catalyst rod decreases only 50 K (from 1173 K to the lowest 1123 K), whereas the temperature gradient dropped by 180 K in the case of conventional DIR-SOFC. From the calculation, the average temperature difference along the DIR-SOFC with inserted catalyst rod was within 8.3 K cm^{-1}, which is lower than the critical point (10 K) as previously reported,[25] whereas the average temperature difference along conventional DIR-SOFC was higher than 20 K. Under these inlet conditions, the output voltage from DIR-SOFC with inserted catalyst rod was 0.74 V, which is higher than that achieved from the conventional DIR-SOFC (0.69 V); furthermore, the electrical efficiency and power density significantly improved (from 45.3 to 63.5% and 0.32 to 0.45 A cm^{-2}). Importantly, the amount of carbon deposition on the anode of DIR-SOFC with inserted catalyst rod was predicted to be significantly less than that of the conventional DIR-SOFC (9.82×10^{-7} g g^{-1} h^{-1} for DIR-SOFC with inserted catalyst rod compared to 3.43×10^{-3} g g^{-1} h^{-1} for conventional DIR-SOFC).

It can be seen that all observed results indicated the great benefit of DIR-SOFC with inserted catalyst rod compared to conventional DIR-SOFC in terms of primary fuel conversion, temperature distribution along the system, electrical efficiency, output power density, and the potential amount of carbon deposition at the anode of SOFC. We suggested that these improvements are mainly related to the presence of higher amount of active nickel in the system, which helps to promote the steam reforming and generate more hydrogen for electrochemical reaction. The reason for better temperature distribution for DIR-SOFC with inserting catalyst rod is also related to the promotion of the endothermic steam reforming of methane to hydrogen, which is simultaneously consumed efficiently by the exothermic electrochemical reaction at SOFC anode. We indicated here that, at steady-state condition where the heat generated from the electrochemical reaction was continuously supplied to the system, the occurring of simultaneous high endothermic steam reforming and exothermic electrochemical reactions results in their good energy exchange coupling, which eventually enhances the great autothermal operation. Regarding the benefit on the reducing of potential carbon deposition at the anode of SOFC, although it was observed from the simulation that some carbon could be formed on the catalyst rod (6.83×10^{-4} g g^{-1} h^{-1}) during operation, this problem can be

Table 3. Constant Parameters for Predicting Activation Loss

ϑ_{anode} (A m^{-2})	5.5×10^8
$\vartheta_{cathode}$ (A m^{-2})	7.0×10^8
$E_{act,anode}$ (kJ $kmol^{-1}$)	1.1×10^5
$E_{act,cathode}$ (kJ $kmol^{-1}$)	1.2×10^5

Table 4. Resistivity of Cell Components, Ni-YSZ/YSZ/LSM[12]

Anode resistance constant	$a = 0.0000298$, $b = -1392$
Cathode resistance constant	$a = 0.0000811$, $b = 600$
Electrolyte resistance constant	$a = 0.0000294$, $b = 10{,}350$

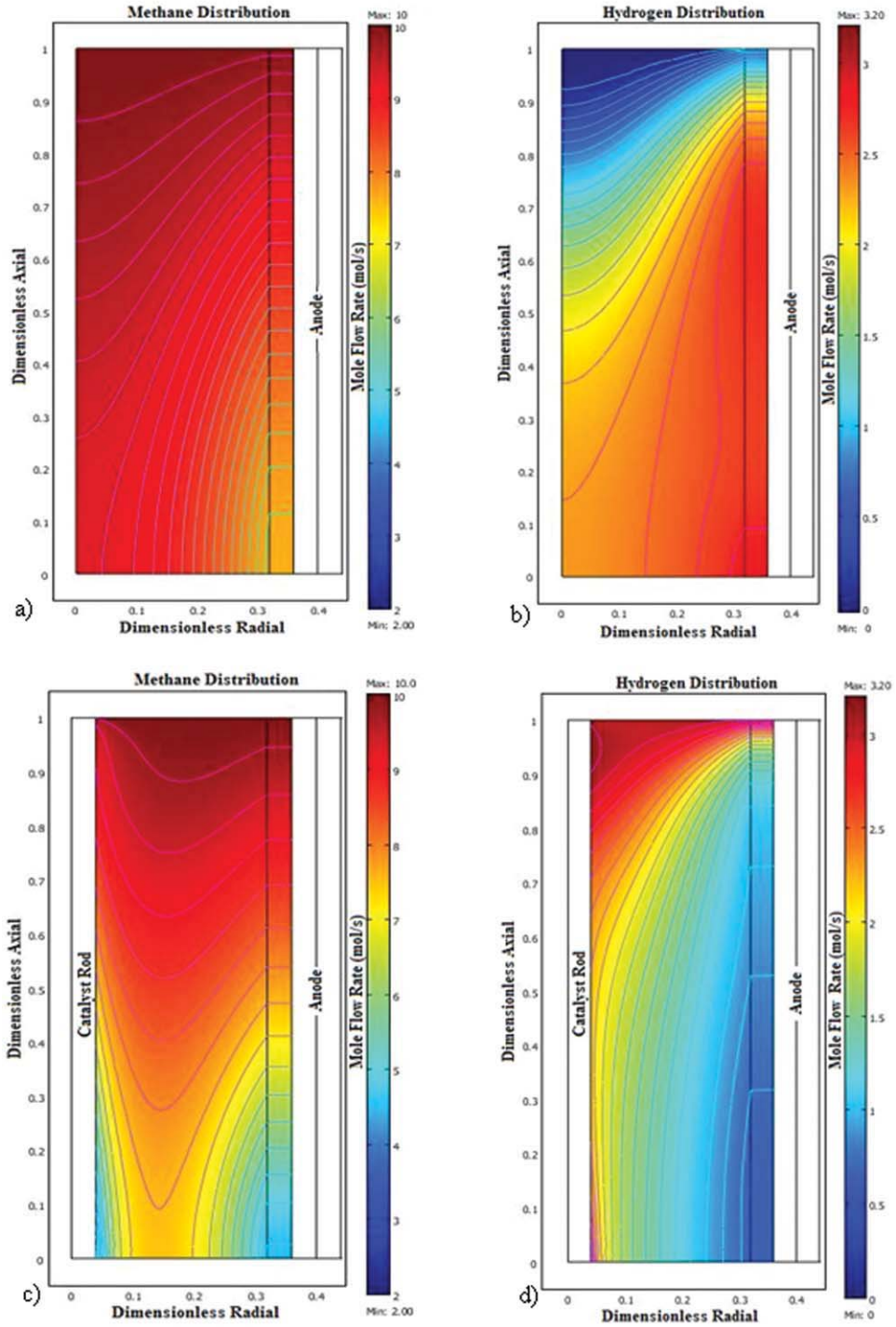

Figure 3. Results from COMSOL® represented the concentration profiles in the fuel channel of DIR-SOFC systems (simulated at 1 bar with inlet *S/C* ratio of 2).

Concentration profiles of (a) methane and (b) hydrogen in the fuel channel in the conventional DIR-SOFC. Concentration profiles of (c) methane and (d) hydrogen in the fuel channel in the inserted catalyst rod DIR-SOFC. [Color figure can be viewed in the online issue, which is available at www.interscience.wiley.com.]

practically minimized by applying alternative reforming catalyst with higher resistance toward carbon deposition (e.g., Rh-based catalysts) without any changing of SOFC anode required; this highlights another beneficial of DIR-SOFC with inserting catalyst rod in terms of catalyst flexibility.

As the next step, the effects of important operating conditions, i.e., inlet fuel flow rate, inlet steam to carbon ratio, and gas flow pattern on the system performance were studied to optimize the suitable operating conditions for these DIR-SOFC systems. It is noted that the effects of other operating

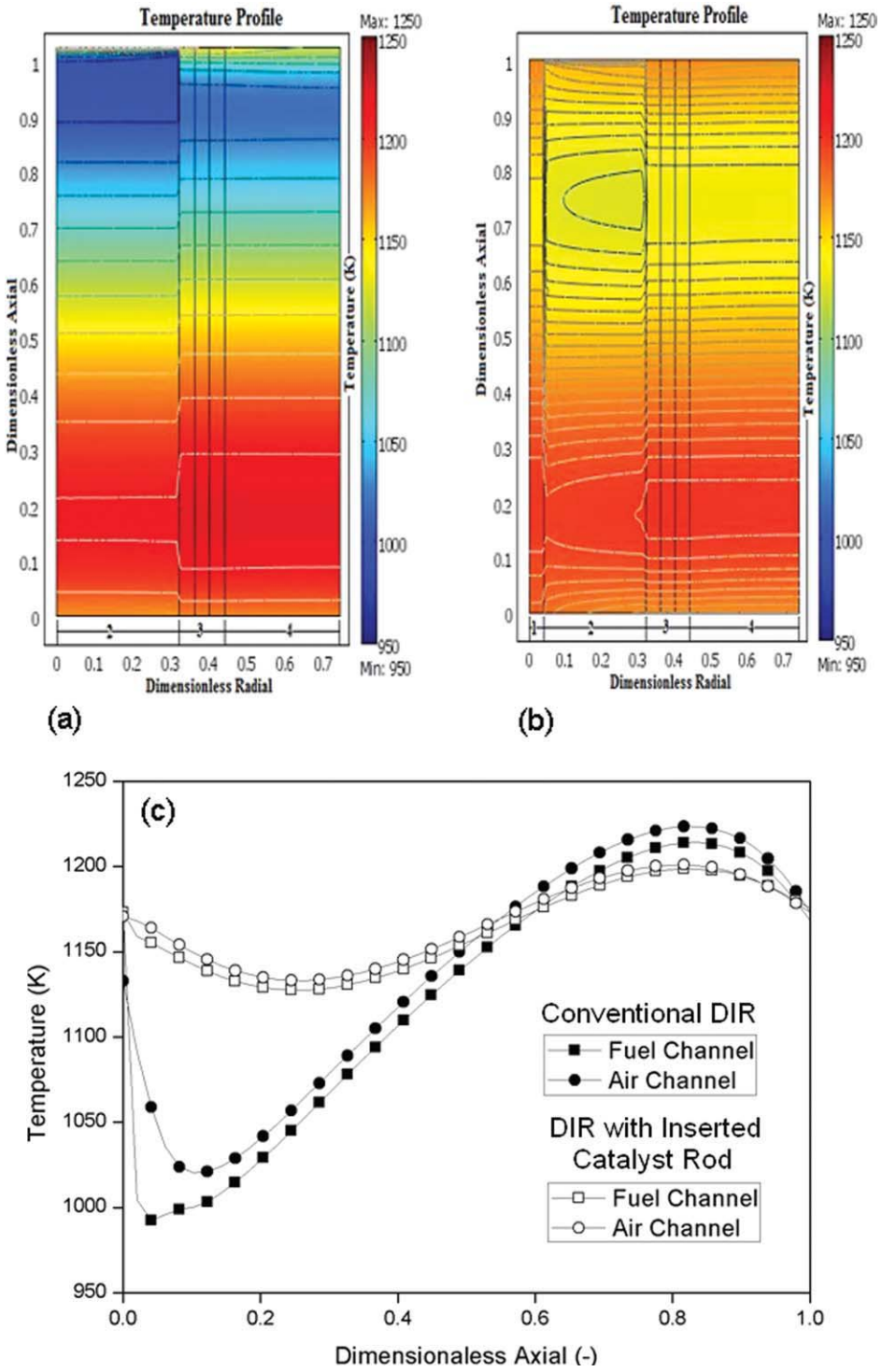

Figure 4. Results from COMSOL® represented the temperature gradient in the fuel and air channels of DIR-SOFC systems (simulated at 1 bar with inlet *S/C* ratio of 2).

Temperature gradients of the fuel and air channels (T_f and T_a, respectively) for (a) conventional DIR-SOFC and (b) inserted catalyst rod DIR-SOFC; (c) comparison of temperature profiles at each channel of both systems. [Color figure can be viewed in the online issue, which is available at www.interscience.wiley.com.]

conditions, e.g., fuel inlet temperature and operating pressure were also carried out. Nevertheless, we found insignificant impact of these operating parameters on the system performance, thus they are not reported here.

Effect of inlet fuel flow rate

The inlet fuel flow rate was found to be one of the major parameters that strongly affects the performance of DIR-SOFC system. Here, the effect of inlet fuel flow rate on the

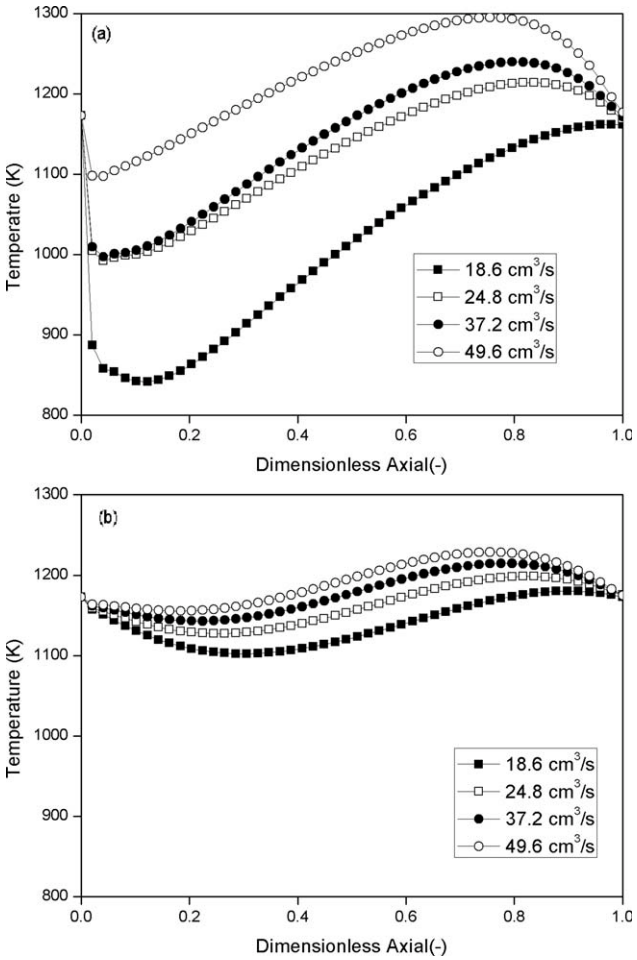

Figure 5. Effect of inlet fuel flow rate on the temperature gradient in the fuel channel of DIR-SOFC systems (simulated at 1 bar with inlet *S/C* ratio of 2).

Temperature profiles in the fuel channel of (a) conventional DIR-SOFC and (b) inserted catalyst rod DIR-SOFC at various inlet fuel flow rates.

temperature gradient, power density, electrical efficiency, and amount of carbon formation for both DIR-SOFC systems was studied by varying the inlet fuel flow rate from 18.6 to 24.8, 37.2, and 49.6 $cm^3\ s^{-1}$. Figure 5a and Table 5 indicate that the cooling effect and power density of conventional DIR-SOFC system can be improved by increasing the inlet fuel flow rate; nevertheless, the electrical efficiency significantly reduced (because of the lower rate of methane conversion at higher fuel flow rate), and the amount of carbon deposition increased considerably. Similar trends were observed for DIR-SOFC with inserted catalyst rod, Figure 5b and Table 5.

Effect of inlet S/C ratio

As possible carbon deposited on the surface of SOFC anode is one of the major problems for DIR-SOFC and it strongly depends on the ratio of steam to carbon in the system, we here aimed at the determination of suitable inlet *S/C* ratio to minimize the potential for carbon deposition in the

Table 5. Effect of Inlet Fuel Flow Rate on the Electrical Efficiency and Power Density of DIR-SOFC Systems (Simulated at 1 bar with Inlet *S/C* Ratio of 2)

	Power Density (A cm^{-2})		Electrical Efficiency (%)	
Inlet Velocity ($cm^3\ s^{-1}$)	Conventional DIR	DIR with Inserted Catalyst	Conventional DIR	DIR with Inserted Catalyst
18.6	0.27	0.42	49.67	78.98
24.8	0.32	0.45	45.25	63.53
37.2	0.36	0.47	33.3	44.64
49.6	0.46	0.51	22.7	35.57

cell and maximize the performance of the system. It is well established that the amount of carbon formation can be efficiently reduced by adding excess steam at the feed; nevertheless, too high steam content can reduce the overall system efficiency because high energy is required to vaporize water to steam. As for the typical methane steam reforming over Ni-based catalysts, it has been reported that the steam to carbon ratio should be in the range of 1.4–3.0.[26] Here, the effect of inlet steam content on the amount of carbon deposition and performance of both DIR-SOFC systems were investigated by varying the inlet steam to carbon (*S/C*) ratios from 1.5 to 4.0.

Figures 6 and 7 and Table 6 present the effect of inlet *S/C* ratio on the temperature gradient along the fuel channel, the electrical efficiency achieved, and the amount of carbon deposition for both DIR-SOFC systems. It can be seen that the amount of carbon formation decreased with increasing inlet *S/C* ratio (Figure 7) because the excess steam can prevent the formation of carbon species from the methane cracking reaction. Nevertheless, considering the temperature gradient and electrical efficiency, it was found that the cooling spot increased with increasing the inlet *S/C* ratio (Figure 6), whereas the electrical efficiency decreased (Table 6). This could be due to the fact that the presence of excess steam diluted hydrogen concentration in the fuel channel and

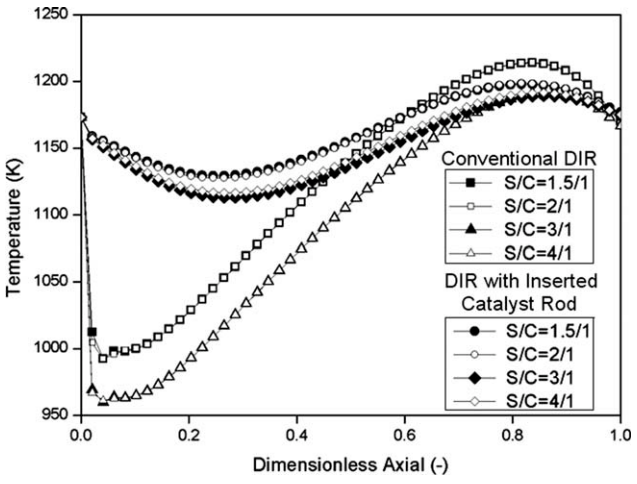

Figure 6. Effect of *S/C* ratio on the temperature gradient in the fuel channel of DIR-SOFC systems (simulated at 1 bar).

Temperature profiles in the fuel channel of conventional DIR-SOFC and inserted catalyst rod DIR-SOFC at various *S/C* ratios.

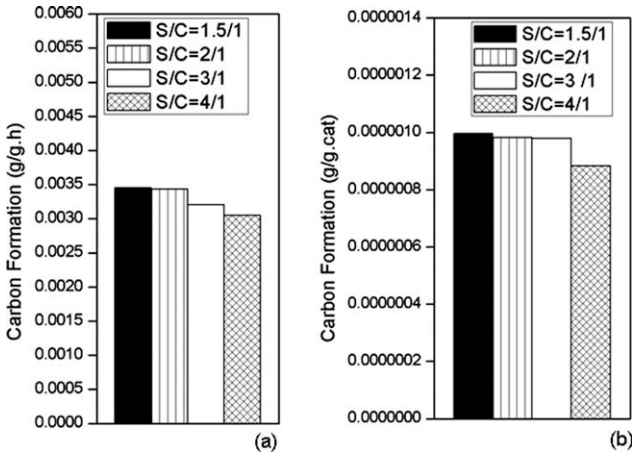

Figure 7. Effect of *S/C* ratio on the predicted carbon formation at the anode of DIR-SOFC systems.

Predicted amount of carbon formation at the anode of (a) conventional DIR-SOFC and (b) inserted catalyst rod DIR-SOFC at various *S/C* ratios.

resulted in lower the exothermic electrochemical reaction; thus, the temperature drops down because of the strong endothermic steam reforming reaction occurred. Hence, we concluded that, to maximize the performance of DIR-SOFC, low inlet *S/C* ratio must be applied; nevertheless, high potential for carbon deposition must be aware. This gains the great benefits of DIR-SOFC with inserted catalyst rod because the rate of carbon deposition was remarkably lower than the conventional DIR-SOFC even at a lower inlet *S/C* ratio (Figure 7b).

The modeling of DIR-SOFC with inserted catalyst rod at particularly low inlet *S/C* ratio (from 2:1 to 0.5:1) was also carried out to determine the optimum operating condition for this system. As shown in Figure 8, the electrical efficiency increased with decreasing inlet *S/C* ratio from 2:1 to 1.1:1, then it rapidly reduced at lower inlet *S/C* ratio; furthermore, significant amount of carbon deposition was observed. These strong negative effects could be due to the incomplete reforming of methane with steam and the occurring of methane cracking instead. Hence, the suitable inlet *S/C* ratio for DIR-SOFC with inserted catalyst rod should be slightly higher than the stoichiometric value (1/1).

Effect of flow direction

For typical autothermal application, e.g., heat exchanging system, flow direction of exchanged fluids strongly affects

Table 6. Effect of Inlet *S/C* Ratio on the Electrical Efficiency and Power Density of DIR-SOFC Systems (Simulated at 1 bar)

	Power Density (A cm^{-2})		Electrical Efficiency (%)	
Steam/ Carbon	Conventional DIR	DIR with Inserted Catalyst	Conventional DIR	DIR with Inserted Catalyst
1.5:1	0.37	0.48	45.95	64.25
2:1	0.32	0.45	45.25	63.53
3:1	0.32	0.41	38.88	47.10
4:1	0.31	0.39	33.99	44.96

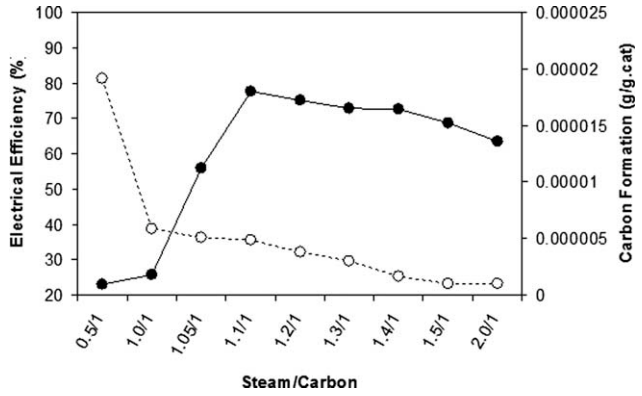

Figure 8. Effect of inlet *S/C* ratio (at lower range) on the electrical efficiency and predicted carbon formation of inserted catalyst rod DIR-SOFC (simulated at 1 bar).

Estimated electrical efficiency and predicted carbon formation at the anode of inserted catalyst rod DIR-SOFC at various *S/C* ratios.

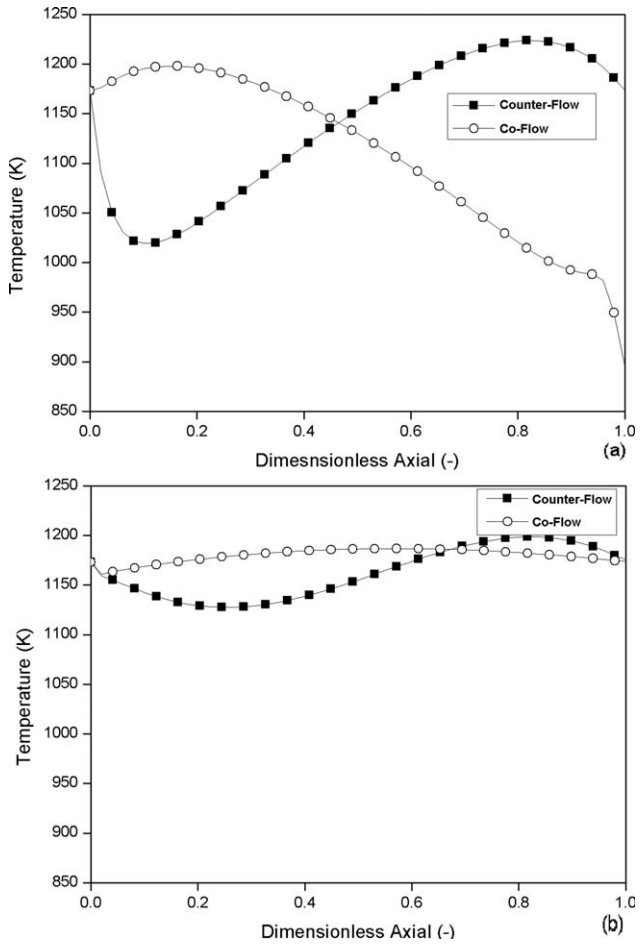

Figure 9. Effect of flow pattern on the temperature gradient in the fuel channel of DIR-SOFC systems (simulated at 1 bar with inlet *S/C* ratio of 2).

Temperature profiles in the fuel channel of (a) conventional DIR-SOFC with co-flow and counter-flow patterns and (b) inserted catalyst rod DIR-SOFC with co-flow and counter-flow patterns.

Table 7. Effect of Flow Pattern on the Electrical Efficiency, Power Density, and Predicted Carbon Formation of DIR-SOFC Systems (Simulated at 1 bar)

Flow Direction	Power Density (A cm^{-2})		Electrical Efficiency (%)		Carbon Formation (g g_{cat}^{-1})	
	Conventional DIR	DIR with Inserted Catalyst	Conventional DIR	DIR with Inserted Catalyst	Conventional DIR	DIR with Inserted Catalyst
Counter-flow	0.32	0.45	45.25	63.53	3.43×10^{-3}	9.82×10^{-7}
Co-flow	0.25	0.51	34.7	71.44	2.83×10^{-3}	9.83×10^{-7}

the heat transfer and reaction behavior in the fluid stream, thus the effect of fuel and oxidant flow direction on the DIR-SOFC performance was also considered here. In the previous sections, air flow is counter-flow to fuel flow in the fuel channel. As an alternative option, the system behavior was analyzed as co-flow pattern by changing mass and energy balances in air channel along with their corresponding boundary conditions while keeping all other operating conditions identical to those of counter-flow pattern. Figures 9a,b show the effect of these two gas flow patterns on the temperature profiles along the fuel channels. It can be seen that the flow directions of fuel gases and air strongly affect the temperature gradient along the system.

In the case of conventional DIR-SOFC configuration with co-flow pattern, no local cooling temperature occurred at the entrance of the fuel channel because the electrochemical reaction occurred rapidly at the entrance of the channel due to the oxygen-rich condition in the air channel, which resulted in sufficient heat for endothermic steam reforming reaction. Nevertheless, this flow pattern caused significant temperature drop at the second half of the channel as most of oxygen was electrochemically consumed, and the required heat for the steam reforming reaction is larger than the generated heat from electrochemical reaction. Under co-flow pattern, the average solid cell temperature was lower than that of the counter-flow pattern and resulted in the increase in cell resistance, which eventually reduced the electrical efficiency (Table 7) and output voltage (reduced by 34.7% to 0.65 V). According to the potential for carbon deposition, it was observed that lower amount of carbon deposition occurred for DIR-SOFC with co-flow pattern, Table 7. This is due to the presence of higher hydrogen content in the fuel channel for DIR-SOFC with co-flow pattern, which reduces the potential for carbon deposition, according to the carbon formation rate expression.[9]

Figure 9b presents the temperature distribution in the fuel channel for DIR-SOFC with inserted catalyst rod under counter- and co-flow patterns. Clearly, DIR-SOFC with co-flow pattern provided smoother temperature distribution with higher average cell temperature. These result in the reducing of cell overpotentials and consequently gain higher output voltage (0.77 V) and electrical efficiency (71.4%, Table 7). It is noted that the flow direction showed insignificant impact on the amount of carbon deposition for DIR-SOFC with inserted catalyst rod (Table 7). We summarized that the high efficiency of DIR-SOFC with inserted catalyst rod under co-flow pattern is due to the good matching between the heat exothermically supplied from the electrochemical reaction and the heat required for the endothermic steam reforming reaction along the fuel cell system, thus concluded here that DIR-SOFC with co-flow pattern is more satisfactory than that with counter-flow pattern.

Conclusions

The simulation indicated that DIR-SOFC with inserted catalyst rod provides smoother temperature gradient along SOFC system with significantly lower local cooling at the entrance of the fuel channel. In addition, higher power density and electrochemical efficiency with less carbon deposition can be achieved compared to the conventional DIR-SOFC.

By increasing the inlet fuel flow rate, the cooling effect and power density of both DIR-SOFC systems can be improved; nevertheless, less electrical efficiency with higher amount of carbon deposition was predicted. It was then found that, to maximize the performance of DIR-SOFC, low inlet *S/C* ratio must be applied; nevertheless, high potential for carbon deposition must be aware. According to the simulation result, the most suitable inlet *S/C* ratio for DIR-SOFC with inserted catalyst rod was 1.1, whereas that of conventional DIR-SOFC should not be less than 1.5. DIR-SOFC with counter-flow pattern was then compared to that with co-flow pattern. In the case of conventional DIR-SOFC, although the local cooling temperature at the entrance of the fuel channel and the amount of carbon deposition can be minimized, this flow pattern caused significant temperature drop at the second half of the channel; furthermore, the average solid cell temperature was lower than that of the counter-flow pattern, which resulted in the increase in cell resistant and eventually reduced the electrical efficient and output voltage. As for DIR-SOFC with inserted catalyst rod, the co-flow pattern provided smoother temperature distribution with higher average cell temperature, which leads to reduced cell overpotentials and consequently higher output voltage and electrical efficiency.

Acknowledgments

The financial support from the Thailand Research Fund (TRF) and Commission on Higher Education, and the Thailand Graduate Institute of Science and Technology (TGIST) program, Thailand's National Science and Technology Development Agency (NSTDA), grant no. TG-55-20-50-058D throughout this project is gratefully acknowledged.

Notation

C_p = specific heat of the gas streams, kJ mol^{-1} K^{-1}
A_{act} = external catalyst surface area = $\frac{\pi(d_t-2\tau_{cat})L}{\pi\left(d_r^2-(d_t-2\tau_{cat})^2\right)L}$
c_i = concentration, mol m^{-3}
$D_{i,j}$ = binary diffusion, m^2 s^{-1}
$D^e_{i,mix}$ = the effective molecular diffusivity, m^2 s^{-1}
$D_{i,ku}$ = the Kundsen diffusivity, m^2 s^{-1}

D_p = pore diameter, m
E = open circuit voltage, V
E_{act} = activation energy, kJ mol^{-1}
F = Faraday's constant, 96,487 C mol^{-1}
ΔH = the change of heat of reaction, kJ mol^{-1}
j_0 = exchange current density, mA cm^{-2}
j = current density, mA cm^{-2}
j_{H_2} = current density from hydrogen oxidation reaction, mA cm^{-2}
h = heat transfer coefficient, kJ m^{-1} s^{-1} K^{-1}
k = thermal conductivity, kJ m^{-1} s^{-1} K^{-1}
N_i^D = the bulk molar diffusive flux of gas component, mol m^{-1} s^{-1}
p^o = standard partial pressure, bar
p_i = partial pressure of species i,
R = universal gas constant; 8.314 J mol^{-1} K^{-1}.
R_{elect} = the hydrogen oxidation reaction rate, mol m^{-2} s^{-1}
q_{rad} = the heat flux from radiation, W m^{-2}
S_{act} = specific surface area of catalyst
T = temperature, K
u = fluid velocity, m s^{-1}
y_i = the mole fraction of gas

Greek letters

ρ = density, kg m^{-3}
γ = special Fuller et al.[17] diffusion volume
ϑ = exchange current density constant, mA cm^{-2}
$\alpha_{a,c}$ = charge transfer coefficient of anode and cathode
σ = Stefan-Boltzmann coefficient
ε = porosity
τ = tortuosity
η_{cell} = voltage drop of the whole cell, Volts
λ = thermal conductivity (kJ m^{-1} s^{-1} K^{-1})

Superscripts

* = active site

Subscripts

a = air channel
c-form = carbon formation
i = component (methanol, water, hydrogen, etc.)
j = reaction (SRM, WGS, etc.)
f = fuel channel
s = solid oxide fuel cell
Act = activation losses
cell = cell stack
con = concentration losses
ohm = ohmic losses
elec = electrochemical reactions
rod = catalyst rod
reform = reforming

Literature Cited

1. Hooger G. *Fuel Cell Technologies Handbook*. Boca Raton, FL: CRC Press, 2003.
2. Larminie J, Dicks A. *Fuel Cell Systems Explained*. Chichester: Wiley, 2000.
3. Angular P, Adjiman CS, Brandon NP. Anode-supported intermediate temperature direct internal reforming solid oxide fuel cell. I. Model-based steady-state performance. *J Power Sources*. 2004;138:120–138.
4. Iora P, Angular P, Adjiman CS, Brandon NP. Comparison of two IT DIR-SOFC models: impact of variable thermodynamic, physical, and flow properties. Steady-state and dynamic analysis. *Chem Eng Sci*. 2005;60:2963–2975.
5. Nikooyeh K, Jeje AA, Hill JM. 3D modeling of anode-supported planar SOFC with internal reforming of methane. *J Power Sources*. 2007;17:601–609.
6. Achenbach E, Riensche E. Methane/steam reforming kinetics for solid oxide fuel cells. *J Power Sources*. 1994;52:283–288.
7. Kandepu R, Imsland L, Foss BA, Stiller C, Thorud B, Bolland O. Modeling and control of a SOFC-GT-based autonomous power system. *Energy*. 2007;32:406–417.
8. Xu J, Froment GF. Methane steam reforming, methanation and water-gas shift. I. Intrinsic kinetics. *AIChE J*. 1989;35:88–96.
9. Zavarukhin SG, Kuvshinov GG. Mathematic modeling of the process of production of nanofibrous carbon from methane in an isothermal reactor with a fixed bed of the Ni-Al_2O_3 catalyst. *Chem Eng J*. 2006;120:139–147.
10. Zhu H, Colclasure AM, Kee RJ, Lin Y, Barnett SA. Anode barrier layers for tubular solid-oxide fuel cells with methane fuel streams. *J Power Sources*. 2006;161:413–419.
11. Costamagna P, Selimovic A, Borghi MD, Agnew G. Electrical model of the integrated planar solid fuel cell (IP-SOFC). *Chem Eng J*. 2004;102:61–69.
12. Chan SH, Khor KA, Xia ZT. A complete polarization model of a solid oxide fuel cell and its sensitivity to the change of cell component thickness. *J Power Sources*. 2001;93:130–140.
13. Leng YJ, Chan SH, Khor KA, Jiang SP. Performance evaluation of anode-supported solid oxide fuel cells with thin film YSZ electrolyte. *Int J Hydrogen Energy*. 2004;29:1025–1033.
14. Xue X, Tang J, Sammes N, Du Y. Dynamic modeling of single tubular SOFC combining heat/mass transfer and electrochemical reaction effects. *J Power Sources*. 2005;142:211–222.
15. Mauri R. A new application of the reciprocity relations to the study of fluid flows through fixed beds. *J Eng Math*. 1998;33:103–112.
16. Todd B, Young JB. Thermodynamic and transport properties of gases for use in solid oxide fuel cell modeling. *J Power Sources*. 2002;110:186–200.
17. Fuller EN, Schettler PD, Giddings JC. A new method for prediction of binary gas-phase diffusion coefficients. *Ind Eng Chem*. 1966;58:19–27.
18. Ramakrishna PA, Yang S, Sohn CH. Innovative design to improve the power density of a solid oxide fuel cell. *J Power Sources*. 2006;158:378–348.
19. Matsuzaki Y, Yasuda I. Relationship between the steady-state polarization of the SOFC air electrode, La0.6Sr0.4MnO3+δ/YSZ, and its complex impedance measured at the equilibrium potential. *Solid State Ionics*. 1999;126:307–313.
20. Zhu H, Kee RJ. A general mathematical model for analyzing the performance of fuel-cell membrane-electrode assemblies. *J Power Sources*. 2003;117:61–74.
21. Zhao F, Virkar AV. Dependence of polarization in anode-supported solid oxide fuel cells on various cell parameters. *J Power Sources*. 2005;141:61–74.
22. Suwanwarangkul R, Croiset E, Fowler MW, Douglas PL, Entche E, Douglas MA. Performance comparison of Fick's, dusty-gas and Stefan-Maxwell models to predict the concentration overpotential of a SOFC anode. *J Power Sources*. 2003;122:9–18.
23. Hernandez-Pacheco E, Singha D, Huttonb PN, Patelb N, Manna MD. A macro-level model for determining the performance characteristics of solid oxide fuel cells. *J Power Sources*. 2004;138:174–186.
24. Stiller C, Thorud B, Seljebø S, Mathisen Ø, Karoliussen H, Bolland O. Finite-volume modeling and hybrid-cycle performance of planar and tubular solid oxide fuel cells. *J Power Sources*. 2005;141:227–240.
25. Lim LT, Chadwick D, Kershenbaum L. Achieving autothermal operation in internally reformed solid oxide fuel cells: simulation studies. *Ind Eng Chem Res*. 2005;44:9609–9618.
26. Yamazaki O, Tomishige K, Fujimoto K. Development of highly stable nickel catalyst for methane-steam reaction under low steam to carbon ratio. *Appl Catal A*. 1996;136:49–56.

Manuscript received Mar. 25, 2009, and revision received Sept. 1, 2009.